frontiers | Frontiers in Energy Research

TYPE Original Research
PUBLISHED 10 October 2023
DOI 10.3389/fenrg.2023.1235721

OPEN ACCESS

EDITED BY
Baskaran Rangasamy,
The Copperbelt University, Zambia

REVIEWED BY
Kailash Venkatraman,
Applied Materials, United States
Hirokazu Munakata,
Tokyo Metropolitan University, Japan

*CORRESPONDENCE
Chiwon Kang,
cwkang@ssu.ac.kr
Byung Hyo Kim,
byunghyokim@ssu.ac.kr

RECEIVED 06 June 2023
ACCEPTED 20 September 2023
PUBLISHED 10 October 2023

CITATION
Kang C, Park Y, Kim Y, Kim SM, Ha S, Yoon HG, Oh KW, Shin K-Y and Kim BH (2023), Solution-processed ZnO coated on $LiNi_{0.8}Mn_{0.1}Co_{0.1}O_2$(NMC811) for enhanced performance of Li-ion battery cathode.
Front. Energy Res. 11:1235721.
doi: 10.3389/fenrg.2023.1235721

Solution-processed ZnO coated on $LiNi_{0.8}Mn_{0.1}Co_{0.1}O_2$(NMC811) for enhanced performance of Li-ion battery cathode

Chiwon Kang[1]*, Yewon Park[2], Yongjoon Kim[1], Soo Min Kim[1], Seungho Ha[1], Hee Gon Yoon[1], Kyu Won Oh[1], Keun-Young Shin[1] and Byung Hyo Kim[1]*

[1]Department of Material Science and Engineering, Soongsil University, Seoul, Republic of Korea, [2]Department of Chemical Engineering, Soongsil University, Seoul, Republic of Korea

The $LiNi_{0.8}Mn_{0.1}Co_{0.1}O_2$ (NMC811) cathode material, widely used in Li-ion batteries (LIBs) for electric vehicles (EVs), has gained a fair amount of attention in the industry due to its advantages of high energy capacity and low production cost. However, during charge-discharge cycles, NMC811 cathode faces issues such as hydrofluoric acid (HF) attack, leaching of transition metals and unstable formation of the cathode electrolyte interphase (CEI), which leads to undermining cathode performance. To address these issues, extensive research has been conducted on coating materials based on metal oxides. In this study, our research team chose Li-doped ZnO (LZO) material, known for its high Li^+ ion conductivity and structural stability. Employing sol-gel synthetic method, we successfully coated LZO material on commercial NMC811 particles, therefore ensuring its coating uniformity through X-ray photoelectron spectroscopy (XPS) and energy-dispersive X-ray spectroscopy energy dispersive spectroscopy analyses. Evaluation of the coated samples (1 wt%, 2 wt%, and 3 wt% LZO on NMC811) revealed their superior electrochemical performance compared to bare NMC811; furthermore, the 2 wt% LZO-coated sample exhibited the highest cycling performance among the coated samples. These findings could be attributed to the lower charge transfer resistance verified by electrochemical impedance spectroscopy (EIS) analysis. Thus, we confirmed the LZO coating layers could provide stability for the NMC811 surface structure, mitigate the leaching of transition metal ions in the NMC811, and promote the formation of an enhanced CEI layer, therefore facilitating Li^+ ion diffusion.

KEYWORDS

sol-gel process, Li-doped ZnO, coating layer, $LiNi_{0.8}Mn_{0.1}Co_{0.1}O_2$(NMC811), cathode materials, Li-ion battery, electric vehicles, large-scale industry

1 Introduction

Li-ion batteries (LIBs) are of paramount importance in the field of electric vehicles (EVs), attracting a significant attention from both industry and academia for commercialization. The development of cathode materials plays a crucial role in the performance enhancement of Li-ion batteries, which requires specific characteristics including: 1) fast charge and discharge capability, 2) higher capacity to increase driving range through high energy density, 3) good mechanical and structural stability for long cycle life, and 4) cost-

effectiveness to promote EV market adoption (Etacheri et al., 2011). To achieve these characteristics, the battery manufacturing industry focuses on two main directions: 1) the development of fundamentally novel cathode materials, which potentially requires several years of research, and 2) the improvement of existing cathode materials through the development of surface coating technologies to optimize material performance (Nisar et al., 2018; Zou et al., 2020).

Recently, as a promising high-performance cathode material, $LiNi_{0.8}Mn_{0.1}Co_{0.1}O_2$(NMC811), has been extensively researched and developed for implementation into EVs by decreasing costly Co content and incorporating higher amount of Ni to achieve cost-effective and high-capacity properties, resulting in a theoretical specific capacity of up to 275 mAh/g (Manthiram et al., 2017). However, the highly reactive Ni^{4+} generation in a NMC811 from the delithiation of Li^+ ion causes side reactions with electrolyte, thus leading to electrode degradation and electrolyte loss. The decrease in Ni^{4+} content forms insulating Ni^{2+}-O^{2-} impurity phases and causes oxygen loss on the surface, deteriorating both crystal structure and cycling stability of NMC811. Owing to the similar ionic radii of Li^+ (0.076 nm) and Ni^{2+} (0.069 nm), Li/Ni cation mixing occurs, therefore inhibiting Li^+ ion diffusion rate and increasing reaction impedance to ultimately result in capacity loss. The anisotropic lattice contraction occurred during charge and discharge cycles induces cracks along grain boundaries and then structural degradation of electrode (Xin et al., 2019). To achieve long-term stability and meet safety requirements, the interface stability between the electrode and electrolyte needs to be improved (Pereira et al., 2020).

There have been numerous reports on coating materials to form protective layers on cathode materials to circumvent a problem with dissolution of transition metal ions in the cathode. In addition, the coating materials can protect the active material from hydrofluoric acid (HF) attack, the result of direct reaction between $LiPF_6$ and moisture in the battery cell (Yang et al., 2006), thus maintaining stable cathode electrolyte interphase (CEI) (Nisar et al., 2021). Oxide-based layered cathode materials (e.g., NMC811) are commonly coated with oxide materials to enhance their electrochemical performance (Nisar et al., 2021; Kaur and Gates, 2022). Coating materials based on metal oxides including Al_2O_3 and ZrO_2 (Zhang et al., 2019), V_2O_5 (Xiong et al., 2013), SnO_2 (Park et al., 2008), ZnO (Chang et al., 2010; Singh et al., 2012; Kong et al., 2014; Qiu et al., 2014), and MgO (Shi et al., 2013), and their excellent features have been reported; however, the coated cathodes exhibit their low reactivity towards Li^+ ion, responsible for low Li^+ ion conductivity. To overcome this shortcoming, Li-doped metal oxides, such as Li_2ZrO_3 (Wu et al., 2015), Li_3VO_4 (Wang et al., 2015), $Li_2Si_2O_5$ (Liu et al., 2016), and $Li_4Ti_5O_{12}$ (Xu et al., 2018), have been strong contenders as effective coating materials for the enhancement in Li^+ ion and electron transport for outstanding battery performance. Coating methods include vapor-phase processes (e.g., atomic layer deposition (ALD) and chemical vapor deposition (CVD)), dry coating processes (e.g., ball milling), and wet chemical processes (e.g., sol-gel, hydrothermal and solvothermal synthesis). The ALD method, which exhibits excellent film conformality, faces limitations in practical large-scale LIB applications due to equipment cost and slow film growth rate (Ahmed et al., 2016). Ball milling possesses an inherent drawback in forming uniform and homogeneous coating layers (Nisar et al., 2021). Thermal and solvent synthesis methods have disadvantages of their requirement of high cost of precursor salts and low product yields, thus interrupting a large-scale industrial application (Zhang et al., 2016). With respect to other synthetic methods, sol-gel process has emerged as an ideal candidate for large-scale production in the industry, as it offers a scalable and efficient manufacturing process, thus leading to the cost-benefit. Additionally, this process provides excellent control over homogeneous mixing of precursor materials at the atomic scale, excellent control of coating stoichiometry, improvement in crystallinity and ability to achieve thin and uniform coatings (Xiong et al., 2013). Nevertheless, the process cost would increase because of the additional drying process of water or other solvents, along with the consequent waste management (Nisar et al., 2021).

In this study, we present a pioneering approach utilizing the sol-gel method to variably modify the thickness and composition of Li-doped ZnO(LZO) thin films for uniform surface coating on commercially available NMC811 cathode material. We also investigate the correlation between optimized battery performance and structural features of LZO coated on NMC811 cathode materials for the application of large-scale LIBs for EVs.

2 Materials and methods

2.1 Synthesis of Li-doped ZnO (LZO) on NMC811 cathode materials

1 g NMC811 particles (Xiamen TOB New Energy Technology) were dispersed in ethanol (2.5 mL) using ultrasonication for 30 min. Then, 0.12 mmol of $Zn(CH_3COO)_2$ (Sigma-Aldrich) and 0.14 mmol of $LiOH{\cdot}H_2O$ (Sigma-Aldrich) precursor materials were added; and then, an additional ethanol (2.5 mL) was added, followed by dispersing the solution with ultrasonication for 30 min. Afterwards, an additional ethanol (45 mL) was added, accompanied by homogeneous mixing with magnetic stirring on a hot plate at 25 °C for 3 h. Subsequently, the ethanol was evaporated during stirring at 50°C for 5 h to produce intermediate product particles. Finally, annealing was conducted at 500 °C for 6 h with a heating rate of 5°C/min to yield LZO on NMC811 cathode materials. To evaluate the influence of Li doping in ZnO on LIB performance, pure ZnO was synthesized using the procedure mentioned above, with the exception of excluding the $LiOH{\cdot}H_2O$ precursor material. Supplementary Figure S1 demonstrates a schematic diagram that illustrates the synthetic procedures of Li-doped ZnO on NMC811 using the sol-gel process.

2.2 Structural analysis

Phases of the as-synthesized LZO on NMC811 cathode materials were identified using powder X-ray diffraction (XRD) analysis using a X-ray diffractometer (XRD, D2 Phaser, Bruker). The surface morphology of the as-synthesized and cycled LZO on NMC 811 cathode materials were analyzed using a field emission scanning electron microscope (FESEM, SmartSEM Sigma, Carl

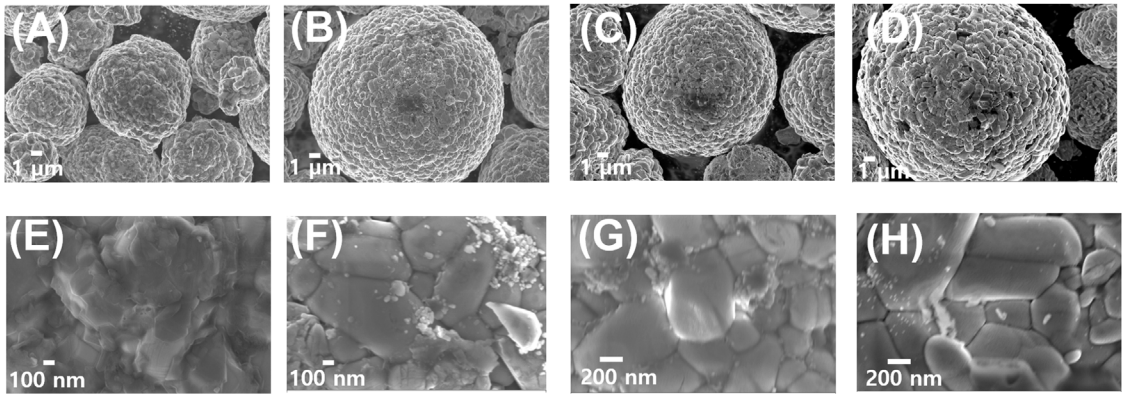

FIGURE 1
SEM images of each sample with the lower and higher magnification for **(A, E)** bare NMC811, **(B, F)** 1 wt% LZO on NMC811, **(C, G)** 2 wt% LZO on NMC811, and **(D, H)** 3 wt% LZO on NMC811.

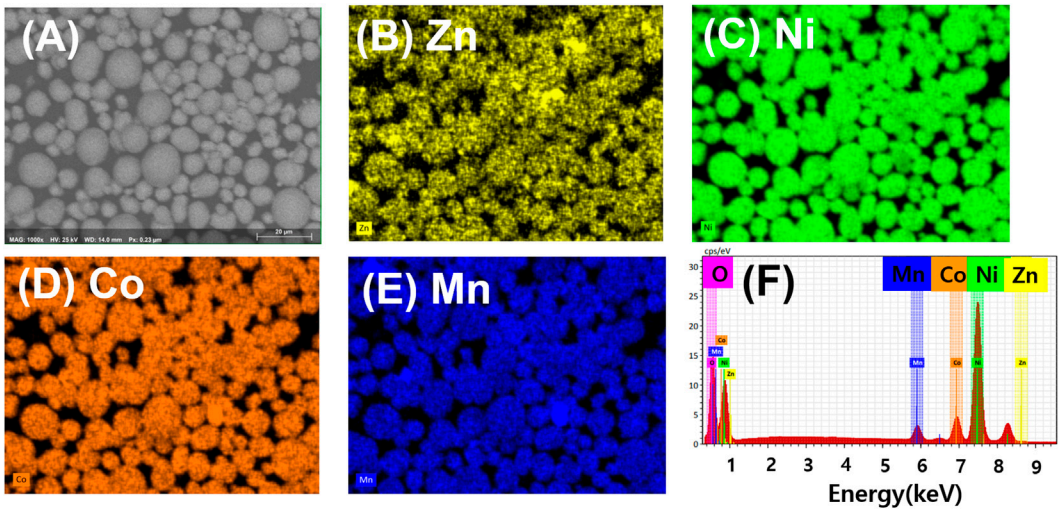

FIGURE 2
EDS color mapping for the 2 wt% LZO on NMC811 sample constituted of each element: **(A)** SEM image of the subjected sample, **(B)** Zn (0.15 at%), **(C)** Ni (33.06 at%), **(D)** Co (5.19 at%), **(E)** Mn (1.95 at%), and **(F)** EDS spectra for each element.

Zeiss). The surface morphology and thickness of the 2 wt% LZO thin layer coated on NMC811, which exhibited the highest LIB performance, were characterized using a 200 kV field emission transmission electron microscope (FE-TEM, JEM-2100F(HR), JEOL). The chemical composition and element distribution of the LZO on NMC811 were examined using energy dispersive X-ray spectroscopy (EDS) with a Bruker Quantax microanalysis system equipped with an XFlash® 6–30 detector. To identify elemental composition and chemical state of materials, X-ray photoelectron spectroscopy (XPS) analysis was conducted (Thermo Scientific Sigma). All spectra were calibrated with the C 1s peak assigned to 284.6 eV. Particularly, peak deconvolution procedures of Ni 2p XPS spectrum and peak-preserving smoothing of Zn 2p XPS spectrum were carried out using Casa XPS software.

2.3 Li-ion battery (LIB) performance

To evaluate the LIB performance of the LZO on NMC811, a slurry was prepared by mixing active material constituted of the LZO on NMC811 (70 wt%) (the NMC811 serves as the active material, while the LZO thin layer plays a role in improving cyclability), conductive additive (20 wt%, Super-P), and binder (10 wt%, poly (vinylidene fluoride) (PVDF)). The mixture was ground for 30 min in a mortar with a pestle; then, N-methyl-2-pyrrolidone (NMP) solution was added. The slurry was cast onto an carbon coated Al foil current collector (MTI Korea) with a doctor blade. Subsequently, the slurry on the current collector was dried at 80°C for 12 h. The disk-type of working electrode was fabricated by a hole punch with 16 mm diameter. We included digital images of the disk-shaped cathode before and after ZnO coating on NMC811 in the Supplementary Figure S2. A CR2032 coin cell was

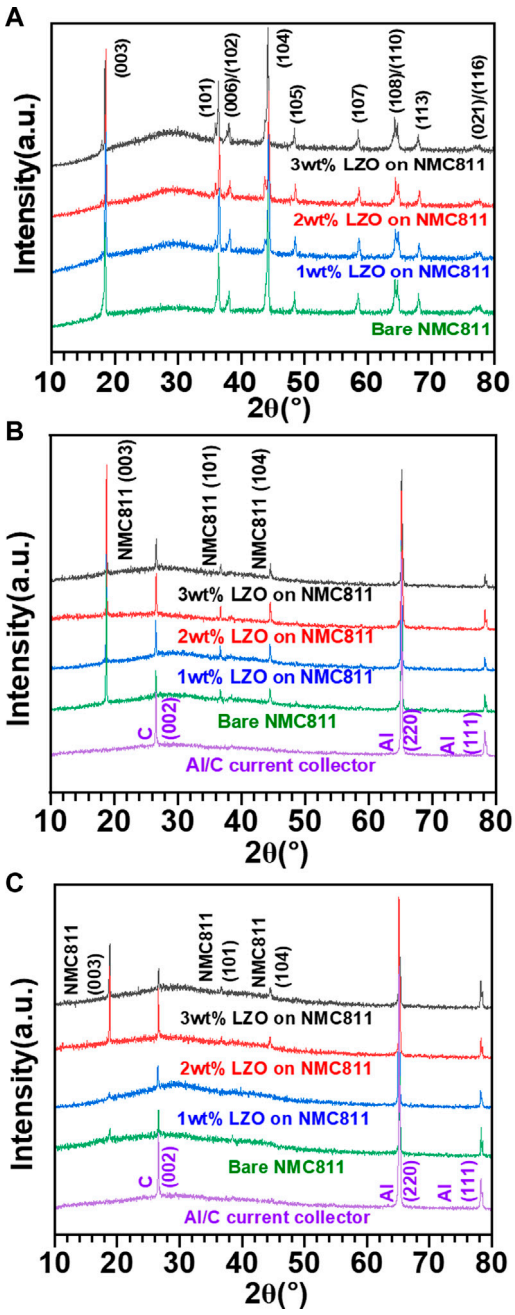

FIGURE 3
XRD patterns of **(A)** powder-type as-synthesized bare NMC811 and LZO coated on NMC811 samples and **(B, C)** slurry electrode-type samples consisting of bare NMC811 and LZO coated on NMC811 as active materials, activated carbon (Super P) and PVDF-based binder in a weight ratio of 8:1:1. Note that panel **(B, C)** represent the comparative XRD patterns of all the samples with different LZO coating conditions before and after LIB test, respectively.

assembled in an Ar-filled glovebox under the extremely low levels of humidity and oxygen of less than 0.1 ppm. As cell components, a Li metal was used as a counter and reference electrode; a polypropylene-polyethylene-polypropylene (PP-PE-PP) trilayer was served as a separator. A 1M $LiPF_6$ in a mixture solvent of ethylene carbonate (EC), ethyl methyl carbonate (EMC), and dimethyl carbonate (DMC) in a volume ratio of 1:1:1 (EC:DMC:EMC) was utilized as an electrolyte. The LIB performance of the LZO on NMC811-based cathode was tested in the coin-cell by using a multi-channel battery testing system (Neware) at 25°C under Galvanostatic mode (constant current density). We also evaluated the cycling performance of an LIB cell with the 2 wt% LZO on NMC811 sample at higher temperature (55°C) for practical application in real LIBs. Additionally, we investigated the thermal stability of LZO coating layer under the elevated temperature. The cell was cycled in the voltage window from 2.7 to 4.4V. After completing 300 cycles, electrochemical impedance spectroscopy (EIS) measurement was conducted on the tested cells using an impedance analyzer (ZIVE MP2; Won-A Tech) at 25 °C. During the EIS measurement, a sinusoidal AC voltage was applied in the frequency range from 1 MHz to 10 mHz with an amplitude of 5 mV. The measurement of transition metal concentrations within the electrolyte employed in the coin cell used for LIB testing was conducted using an inductively coupled plasma mass spectrometer (ICP-MS, Agilent 7900 ICP-MS).

3 Results and discussion

3.1 Structural analysis

Figure 1 presents the surface morphology of bare NMC811 particles and NMC811 particles coated with Li-doped ZnO (LZO) at ratios of 1, 2, and 3 wt% using the sol-gel synthetic method. Figures 1A, E depict images captured at the lower and higher magnifications, respectively. Upon coating, insignificant changes in particle shape and size are observed, indicating that LZO is uniformly and thinly coated on the surface of NMC811 without altering its surface characteristics. The spherical particles have an approximate size of 10 μm, comprising agglomerated nano-sized primary particles with a length of approximately 500 nm (Xu et al., 2021). This meatball-like structure provides a higher tap density, crucial for achieving superior electrochemical performance compared to other dispersed particle structures. Furthermore, we measured a thickness of 3–5 nm for a 2 wt% LZO thin layer coated on NMC811 using TEM analytical technique for both bare NMC811 and the 2 wt% LZO-coated NMC811 particulate samples (see Supplementary Figure S3).

Successful coating of ZnO on NMC811 is confirmed by EDS color mapping. In Figure 2, the color mapping and spectra obtained through energy dispersive spectroscopy (EDS) display the distribution of various elements (Zn, Ni, Co, O, and Mn) present on the surface of NMC811 particles coated with LZO. The EDS analysis reveals that all the elements in LZO on NMC811 are uniformly distributed across all the particles. Noticeably, Figure 2B confirms the uniform coating of Zn element on the surface of NMC811 particles. These results clearly demonstrate the presence of uniformly coated Li-doped ZnO on the surface of NMC811 particles. According to the EDS spectra (Figure 2F), Zn exhibits a composition of approximately 0.15 at%, while the atomic ratio of Zn was recorded as a value of zero for the bare NMC811. Through EDS data, we can confirm that LZO synthesized via a mass-producible and highly-efficient sol-gel synthetic method could be uniformly and effectively coated on commercially available NMC811 cathode particles.

As shown in Figure 3, the diffraction peaks can be correlated to the hexagonal a-$NaFeO_2$ structure with the R-3m space group in the absence of any additional diffraction peaks associated with

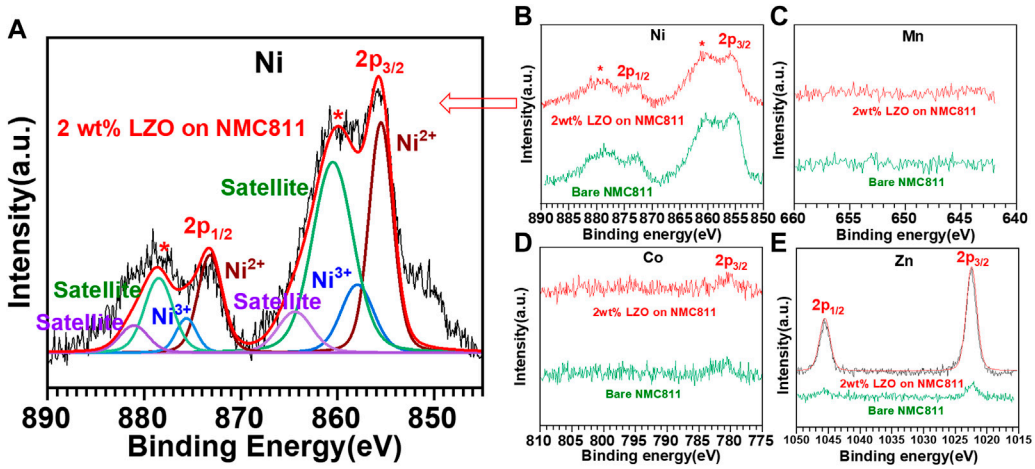

FIGURE 4
XPS spectra data of the bare NMC811 and the 2 wt% LZO on NMC811 samples: **(A, B)** deconvoluted, raw and peak-preserving smoothing data of Ni 2p (55.41 at%), **(C)** raw data of Mn 2p (3.42 at%), **(D)** raw data of Co 2p (10.36 at%) and **(E)** raw and peak-preserving smoothing data of Zn 2p (30.81 at%).

secondary phases or impurities. The separation of peak pairs (006)/(102) and (108)/(110) in all the samples indicates the formation of a layered structure (Yang et al., 2012). Furthermore, the LZO coating material has only a miniscule impact on the NMC811 cathode structure. Considering samples under all conditions before conducting battery cycling test, we can observe peaks corresponding to the crystalline planes of NMC811 including (003) at 18.8°, (101) at 36.7° and (104) at 44.5° (Figure 3B). In contrast, among the samples subjected to the LIB test up to 300 cycles (Figure 3C), we can only identify peaks related to the crystalline planes of NMC811 from the samples coated with 2 and 3 wt% LZO. This suggests that coating materials with a thickness of at least 2 wt% could effectively maintain the structural integrity of the crystalline planes of the cycled NMC811 samples. Nevertheless, we could find no peak regarding $Zn_{1-x}Li_xO$ ($0.00 \leq x \leq 0.50$) phases with a wurtzite hexagonal structure (JCPDS card (ID-36–1,451)) (Lin et al., 2010; Ardyanian and Sedigh, 2014; Rakkesh and Balakumar, 2014). This finding demonstrates there is a limitation in obtaining XRD patterns for LZO, which is attributed to low-energy X-ray source in a laboratory-scale XRD equipment, particularly for detecting thin coating layers with sub-nanometer grain size.

Figure 4 shows the results of XPS surface analysis for the electrodes fabricated with bare NMC811 and 2 wt% LZO on NMC811 particles, which exhibits the best battery performance. For Ni in both samples (Figures 4A, B), we can acquire peaks corresponding to Ni $2p_{3/2}$ and Ni $2p_{1/2}$ binding energies at 855.8 and 872.7 eV, respectively (Yu et al., 2022). For the 2wt% LZO on NMC811 sample (Figure 4A), the Ni $2p_{3/2}$ binding energy peak can be deconvoluted into two components located at 855.5 and 858 eV, respectively, which are consistent with the binding energies of Ni^{3+} and Ni^{2+}, indicating a mixed state of Ni^{2+} and Ni^{3+} oxidation states near the surface of particles. Similarly, the Ni $2p_{1/2}$ binding energy peak can be deconvoluted into two components located at Ni^{2+} (873.2 eV) and Ni^{3+} (875.6 eV) (Kong et al., 2014). In contrast, for Mn with a lower composition (Figure 4C), there is insignificant peak corresponding to Mn $2p_{3/2}$ and Mn $2p_{1/2}$ binding energies at 642.5 and 654 eV, respectively (Pereira et al., 2020). Similarly, for Co with a lower composition (Figure 4D), we can attain a small broad peak corresponding to Co $2p_{3/2}$ binding energy at 781 eV (Fantauzzi et al., 2019). Our main interest lies in determining whether LZO is uniformly coated on the surface of NMC811 particles through XPS analysis. Figure 4E shows the observation of peaks corresponding to Zn (1,022.7 eV for Zn $2p_{3/2}$ and 1,045.9 eV for Zn $2p_{1/2}$) for the 2 wt% LZO on NMC811, thus manifesting the presence of Zn-O chemical bonding in ZnO. Based on the spectrum, Zn shows a composition of 30.81 at%. These findings can justify the formation of LZO coating materials on the surface of NMC811 (Kong et al., 2014). In contrast, we could find insignificant Zn element detected for the bare NMC811 cathode material as illustrated in Figure 4E.

3.2 Li-ion battery performance

Figure 5A presents the voltage profiles of the 2 wt% LZO on NMC811/Li half-cell during the initial two cycles between 4.4V and 2.7V at 25°C. The half-cell exhibits charge capacities of 239.3 and 208.1 mAh/g and discharge capacities of 205.5 and 204.8 mAh/g in the first and second cycle, respectively. Coulombic efficiencies (CE) of the first and second cycles are recorded as 85.9% and 99.7%, respectively. To compare, CE of the bare NMC811 for the first and second cycles are measured as 81.2% and 97.5%, respectively (see Supplementary Figure S4). The superior CE values of 2 wt% LZO on NMC811 is attributed by a process of formation and stabilization of the solid electrolyte interface (SEI) protective layer (Nisar et al., 2021). Figure 5B displays the cycle performance results obtained from the cell measurements of the bare NMC811 and the LZO coated on NMC811 samples, with LZO content controlled at 1, 2, and 3 wt% with respect to bare NMC811. Measurements were conducted four times for each sample at 25°C; then, the average value of each one was calculated and presented in Figure 5B. Noticeably, all samples showed a decrease in specific capacity with increasing cycle number. When cycled up to 300 cycles, the

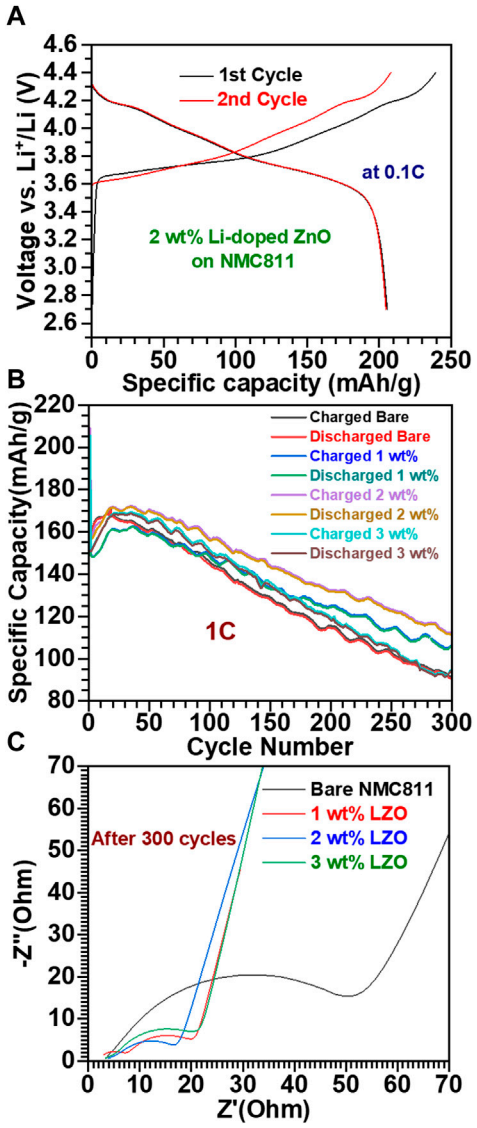

FIGURE 5
LIB peformance of the bare NMC811 and LZO-coated on NMC811 samples: **(A)** voltage profiles of the 2 wt% LZO on NMC811 sample for initial two charge and discharge cycles, **(B)** comparative cycling performance of the different samples and **(C)** EIS data for the different samples tested up to 300 cycles.

bare NMC811 cathode material delivers a capacity of approximately 90 mAh/g with a capacity retention of 59%. Among the LZO on NMC811 samples, the 2 wt% sample demonstrated the highest capacity (approximately 112 mAh/g) and a capacity retention of approximately 71%, superior to the results of other oxide-coated NMC811 (Himani et al., 2021; Jia et al., 2022). In comparison, the 1 and 3 wt% samples show capacities of 107 mAh/g and 95 mAh/g, respectively, with capacity retentions of nearly 71% and 63%, respectively. Based on these results, we could confirm that LZO coating materials guard the active material against HF attack, mitigate a problem with the leaching of transition metal ions in the cathode during cycling, and maintain a stable cathode electrolyte interphase (CEI) (Nisar et al., 2021). We also evaluated the cycling performance of an LIB cell with a 2 wt% LZO on NMC811 sample at a higher temperature (55°C) for practical applications in real LIBs. Supplementary Figure S5 demonstrates the superior LIB performance observed at higher temperature compared to lower temperature (25°C). Based on this result, we can confirm the excellent thermal stability of the LZO coating layer under elevated temperatures.

As mentioned in the introduction section, we doped Li into the ZnO structure to enhance the low Li^+ ion conductivity of the pure ZnO coating layer. To ascertain the successful incorporation of Li^+ ions into the ZnO structure, the conventional approach in previous reports have involved analyzing the presence of Li within Li-doped ZnO using XPS (Xiaofeng et al., 2019; Jie et al., 2022). However, we faced a limitation to apply this approach to our proposed Li-doped ZnO coating layer in this study. Both NMC811 and 3–5 nm thick LZO thin film coated on NMC811 samples contain Li; therefore, data obtained from analytical techniques can indicate the presence of Li in both NMC811 and LZO on NMC811. As an alternative approach to analytical techniques, we compared the electrochemical performance between 2 wt% ZnO on NMC811 and 2 wt% Li-doped ZnO on NMC811 at 1C for 10 cycles to imply the presence of Li within the ZnO structure in the LZO sample (Supplementary Figure S6). The specific capacity of the 2 wt% LZO on NMC811 surpasses that of 2 wt% ZnO on NMC811 for all the cycles. These data demonstrate that Li should be doped into ZnO and act as a facilitator for Li^+ ion and electron transport, leading to superior LIB performance compared to pure ZnO.

Furthermore, through 300 charge-discharge cycling test, a reduction in capacity retention is observed in all samples as the cycles increase. This phenomenon can be attributed to the dissolution of transition metals within NMC811 and the structural degradation of NMC811 during cycling processes (Nisar et al., 2021). Noticeably, our proposed LZO coating layer serves as a protective barrier to mitigate these issues. To verify this hypothesis, post-mortem analyses (SEM and ICP-MS) were performed on both bare NMC811 and 2 wt% LZO on NMC811 after completing the charge-discharge testing. As illustrated in Supplementary Figure S7, we observe distinct morphological differences between bare NMC811 and 2 wt% LZO on NMC811 in the SEM images. This observation confirms that the structural integrity of 2 wt% LZO on NMC811 is more preserved compared to that of bare NMC811. Furthermore, ICP-MS analysis was employed to determine the concentrations of Ni, Co, and Mn, the transition metal constituents of NMC811. For bare NMC811, the concentrations of Ni, Co, and Mn are 460, 45, and 68 ppb, respectively. In contrast, for 2 wt% LZO on NMC811, the corresponding concentrations are 370, 46, and 70 ppb, respectively. This higher Ni concentration in bare NMC811 indicates a greater amount of Ni dissolution from bare NMC811 compared to 2 wt% LZO on NMC811. These findings demonstrate the significant role of the LZO coating layer in mitigating the structural degradation of NMC811 and suppressing the leaching of transition metals into the electrolyte during cycling, in line with the LIB performance exhibited in Figure 5B.

To further evaluate the effect of LZO coating materials on NMC811 cathodes, we conducted electrochemical impedance spectroscopy (EIS) analysis. Figure 5C presents the Nyquist plots obtained for each sample after 300 cycle test. A slight interruption at high frequency corresponds to the electrolyte resistance (R_s), which lies within the range of 3–4 Ω for all samples. As the frequency changes from high to medium regions, the charge transfer resistance (R_{ct}) can be

calculated for each sample based on the semicircle. The values of R_{ct} for each sample follow the sequence: 16.7 Ω (2 wt% LZO), 20 Ω (1 wt% LZO), 20.2 Ω (3 wt% LZO), and 50.7 Ω (bare NMC811). It should be noted that the smaller values of R_{ct} for all the LZO on NMC811 samples than the bare NMC811 sample can be mainly associated with the significant roles of LZO on NMC811 as mentioned earlier (Song et al., 2011; Shi et al., 2013; Kong et al., 2014). These results are consistent with the aforementioned LIB performance during charge and discharge cycles (see Figure 5B). Moreover, the calculated Li^+ diffusion coefficient for the bare NCM811 electrode subjected to 300 cycling test is 2.34×10^{-15} cm^2/s, while those for the NCM811 samples with 1 wt %, 2 wt%, and 3 wt% LZO coatings are 1.31×10^{-14} cm^2/s, 1.99×10^{-14} cm^2/s, and 4.66×10^{-15} cm^2/s, respectively (Feng et al., 2022). These results confirm that the LZO coating layer can enhance Li^+ ion kinetics, consistent with the LIB performance at 1 C for 300 cycles (Figure 5B) and previous reports (Tongxin et al., 2022).

4 Conclusion

The NMC811 cathode materials have gained the spotlight to be implemented into the LIBs for EVs owing to their main features of high specific capacity and low production cost. However, these materials have faced the technical challenge of their vulnerability to HF attack, leaching of transition metals and the formation of unstable cathode electrolyte interphase (CEI) layers; therefore, resulting in LIB performance degradation during charge and discharge cycles. The surface modification of NMC811 by metal oxide-based coating materials could be a viable way to solve this challenge. In this study, we selected LZO coating material, which has a high Li^+ ion conductivity and excellent structural stability. The commercial NMC811 particles were coated using the sol-gel synthetic method, which has a high potential for industrial-scale applications. We could confirm the uniformity of the LZO coating materials and their uniform distribution on the entire surface of the NMC811 particles through XPS and EDS analyses. Furthermore, we evaluated LIB performance for different samples (e.g., bare NMC811, 1, 2, and 3 wt% LZO on NMC811). The results demonstrated superior battery performance of the coated samples to the bare NMC811 counterpart; especially, the 2 wt% LZO on NMC811 exhibited the highest cycling performance. This observation was in line with the results from EIS analysis. Thus, we confirm that the LZO could provide a stable surface structure for the NMC811 cathode materials, suppress the leaching of transition metal ions, and promote the formation of an optimized CEI layer, thus facilitating Li^+ ion diffusion. With such impressive LIB performance and structural characteristics, our proposed LZO thin layer coated on NMC811 has the potential to drive technological innovation in the development of advanced, large-scale LIBs for EVs.

Data availability statement

The original contributions presented in the study are included in the article/Supplementary Material, further inquiries can be directed to the corresponding authors.

Author contributions

Conceptualization, CK and BK; methodology, CK, YP, YK, SK, SH, K-YS, and BK; formal analysis, CK and BK; investigation, CK and BK; resources, CK and BK; data curation, CK, SK, HY, and KO; writing—original draft preparation, CK; writing—review and editing, CK and BK; visualization, CK; supervision, CK and BK; project administration, CK and BK; funding acquisition, CK and BK. All authors contributed to the article and approved the submitted version.

Funding

This research was funded by National Research Foundation of Korea (NRF) with grant numbers of NRF-2021R1C1C1014339 and NRF-2020R1I1A1A01068549. This research was also supported by the Alchemist project (NTIS No. 1415187370 and KEIT No. 20025757) of Ministry of Trade, Industry and Energy (MOTIE, Korea).

Conflict of interest

The authors declare that the research was conducted in the absence of any commercial or financial relationships that could be construed as a potential conflict of interest.

Publisher's note

Supplementary material

The Supplementary Material for this article can be found online at: https://www.frontiersin.org/articles/10.3389/fenrg.2023.1235721/full#supplementary-material

References

Ahmed, B., Xia, C., and Alshareef, H. N. (2016). Electrode surface engineering by atomic layer deposition: A promising pathway toward better energy storage. *Nano Today* 11 (2), 250–271. doi:10.1016/j.nantod.2016.04.004

Ardyanian, M., and Sedigh, N. (2014). Heavy lithium-doped ZnO thin films prepared by spray pyrolysis method. *Bull. Mater. Sci.* 37, 1309–1314. doi:10.1007/s12034-014-0076-4

Chang, W., Choi, J.-W., Im, J.-C., and Lee, J. K. (2010). Effects of ZnO coating on electrochemical performance and thermal stability of $LiCoO_2$ as cathode material for lithium-ion batteries. *J. Power Sources* 195 (1), 320–326. doi:10.1016/j.jpowsour.2009.06.104

Etacheri, V., Marom, R., Elazari, R., Salitra, G., and Aurbach, D. (2011). Challenges in the development of advanced Li-ion batteries: A review. *Energy and Environ. Sci.* 4 (9), 3243–3262. doi:10.1039/c1ee01598b

Fantauzzi, M., Secci, F., Angotzi, M. S., Passiu, C., Cannas, C., and Rossi, A. (2019). Nanostructured spinel cobalt ferrites: fe and Co chemical state, cation distribution and

size effects by X-ray photoelectron spectroscopy. *RSC Adv.* 9 (33), 19171–19179. doi:10.1039/c9ra03488a

Feng, W., Yikuan, L., Peng, L., Muhammad-Sadeeq, B., Jianqiu, D., and Zhongmin, W. (2022). Improved cycling performance and high rate capacity of $LiNi_{0.8}Co_{0.1}Mn_{0.1}O_2$ cathode achieved by $Al(PO_3)_3$ modification via dry coating ball milling. *Coatings* 12 (3), 319. doi:10.3390/coatings12030319

Himani, G., Shishir, K. S., Nitin, S., Dipika, M., Rupesh, K. T., Raghvendra, M., et al. (2021). Improved high voltage performance of Li-ion conducting coated Ni-rich NMC cathode materials for rechargeable Li battery. *ACS Appl. Energy Mater.* 4 (12), 13878–13889. doi:10.1021/acsaem.1c02681

Jia, Y., Keliang, R., Mingzi, H., Ting, W., Dan, W., Tongshuai, W., et al. (2022). New insight into lattice variations of Ni-rich NMC811 cathode induced by Li_2ZrO_3 coating. *Mater. Technol.* 37 (11), 1926–1935. doi:10.1080/10667857.2021.2009095

Jie, W., Hailin, P., Xiaoyun, X., Hui, J., Wenjia, M., Shaobing, X., et al. (2022). Li-doped ZnO electron transport layer for improved performance and photostability of organic solar cells. *ACS Appl. Mater. Interfaces* 14 (10), 12450–12460. doi:10.1021/acsami.1c22093

Kaur, G., and Gates, B. D. (2022). Review—surface coatings for cathodes in lithium ion batteries: from crystal structures to electrochemical performance. *J. Electrochem. Soc.* 169 (4), 043504. doi:10.1149/1945-7111/ac60f3

Kong, J.-Z., Ren, C., Tai, G.-A., Zhang, X., Li, A.-D., Wu, D., et al. (2014). Ultrathin ZnO coating for improved electrochemical performance of LiNi0. 5Co0. 2Mn0. 3O2 cathode material. *J. Power Sources* 266, 433–439. doi:10.1016/j.jpowsour.2014.05.027

Lin, Y.-J., Wang, M.-S., Liu, C.-J., and Huang, H.-J. (2010). Defects, stress and abnormal shift of the (0 0 2) diffraction peak for Li-doped ZnO films. *Appl. Surf. Sci.* 256 (24), 7623–7627. doi:10.1016/j.apsusc.2010.06.016

Liu, S., Wu, H., Huang, L., Xiang, M., Liu, H., and Zhang, Y. (2016). Synthesis of Li2Si2O5-coated LiNi0. 6Co0. 2Mn0. 2O2 cathode materials with enhanced high-voltage electrochemical properties for lithium-ion batteries. *J. Alloys Compd.* 674, 447–454. doi:10.1016/j.jallcom.2016.03.060

Manthiram, A., Song, B., and Li, W. (2017). A perspective on nickel-rich layered oxide cathodes for lithium-ion batteries. *Energy Storage Mater.* 6, 125–139. doi:10.1016/j.ensm.2016.10.007

Nisar, U., Amin, R., Essehli, R., Shakoor, R., Kahraman, R., Kim, D. K., et al. (2018). Extreme fast charging characteristics of zirconia modified LiNi0. 5Mn1. 5O4 cathode for lithium ion batteries. *J. Power Sources* 396, 774–781. doi:10.1016/j.jpowsour.2018.06.065

Nisar, U., Muralidharan, N., Essehli, R., Amin, R., and Belharouak, I. (2021). Valuation of surface coatings in high-energy density lithium-ion battery cathode materials. *Energy Storage Mater.* 38, 309–328. doi:10.1016/j.ensm.2021.03.015

Park, S. B., Shin, H. C., Lee, W.-G., Cho, W. I., and Jang, H. (2008). Improvement of capacity fading resistance of $LiMn_2O_4$ by amphoteric oxides. *J. Power Sources* 180 (1), 597–601. doi:10.1016/j.jpowsour.2008.01.051

Pereira, J. A., Lacerda, J. N., Coelho, I. F., de Sc Nogueira, C., Franceschini, D. F., Ponzio, E. A., et al. (2020). Tuning the morphology of manganese oxide nanostructures for obtaining both high gravimetric and volumetric capacitance. *Mater. Adv.* 1 (7), 2433–2442. doi:10.1039/d0ma00524j

Qiu, B., Wang, J., Xia, Y., Wei, Z., Han, S., and Liu, Z. (2014). Enhanced electrochemical performance with surface coating by reactive magnetron sputtering on lithium-rich layered oxide electrodes. *ACS Appl. Mater. interfaces* 6 (12), 9185–9193. doi:10.1021/am501293y

Rakkesh, R. A., and Balakumar, S. (2014). Structural, electrical transport and optical studies of Li ion doped ZnO nanostructures. *Process. Appl. Ceram.* 8 (1), 7–13. doi:10.2298/pac1401007r

Shi, S., Tu, J., Tang, Y., Liu, X., Zhang, Y., Wang, X., et al. (2013). Enhanced cycling stability of Li [Li0. 2Mn0. 54Ni0. 13Co0. 13] O2 by surface modification of MgO with melting impregnation method. *Electrochimica Acta* 88, 671–679. doi:10.1016/j.electacta.2012.10.111

Singh, G., Thomas, R., Kumar, A., Katiyar, R., and Manivannan, A. (2012). Electrochemical and structural investigations on ZnO treated 0.5 Li_2MnO_3-0.5 $LiMn_{0.5}Ni_{0.5}O_2$ layered composite cathode material for lithium ion battery. *J. Electrochem. Soc.* 159 (4), A470–A478. doi:10.1149/2.100204jes

Song, H. G., Kim, J. Y., Kim, K. T., and Park, Y. J. (2011). Enhanced electrochemical properties of Li $(Ni_{0.4}Co_{0.3}Mn_{0.3})O_2$ cathode by surface modification using Li_3PO_4-based materials. *J. Power Sources* 196 (16), 6847–6855. doi:10.1016/j.jpowsour.2010.09.027

Tongxin, L., Donglin, L., Qingbo, Z., Jianhang, G., Long, Z., and Xiaojiu, L. (2022). Improving fast charging-discharging performances of Ni-rich $LiNi_{0.8}Co_{0.1}Mn_{0.1}O_2$ cathode material by electronic conductor $LaNiO_3$ crystallites. *Materials* 15 (1), 396. doi:10.3390/ma15010396

Wang, W., Yin, Z., Wang, Z., Li, X., and Guo, H. (2015). Effect of heat-treatment on electrochemical performance of Li3VO4-coated LiNi1/3Co1/3Mn1/3O2 cathode materials. *Mater. Lett.* 160, 298–301. doi:10.1016/j.matlet.2015.07.160

Wu, H., Wang, Z., Liu, S., Zhang, L., and Zhang, Y. (2015). Fabrication of Li+-Conductive Li2ZrO3-based shell encapsulated LiNi0. 5Co0. 2Mn0. 3O2 microspheres as high-rate and long-life cathode materials for Li-ion batteries. *ChemElectroChem* 2 (12), 1921–1928. doi:10.1002/celc.201500303

Xiaofeng, Z., Yi, L., Chunpeng, A., and Dianzhong, W. (2019). Resistive switching characteristics of Li-doped ZnO thin films based on magnetron sputtering. *Materials* 12 (8), 1282. doi:10.3390/ma12081282

Xin, F., Zhou, H., Chen, X., Zuba, M., Chernova, N., Zhou, G., et al. (2019). Li–Nb–O coating/substitution enhances the electrochemical performance of the LiNi0. 8Mn0. 1Co0. 1O2 (NMC 811) cathode. *ACS Appl. Mater. interfaces* 11 (38), 34889–34894. doi:10.1021/acsami.9b09696

Xiong, X., Wang, Z., Guo, H., Zhang, Q., and Li, X. (2013). Enhanced electrochemical properties of lithium-reactive V_2O_5 coated on the $LiNi_{0.8}Co_{0.1}Mn_{0.1}O_2$ cathode material for lithium ion batteries at 60°C. *J. Mater. Chem. A* 1 (4), 1284–1288. doi:10.1039/c2ta00678b

Xu, C., Märker, K., Lee, J., Mahadevegowda, A., Reeves, P. J., Day, S. J., et al. (2021). Bulk fatigue induced by surface reconstruction in layered Ni-rich cathodes for Li-ion batteries. *Nat. Mater.* 20 (1), 84–92. doi:10.1038/s41563-020-0767-8

Xu, Y.-D., Xiang, W., Wu, Z.-G., Xu, C.-L., Li, Y.-C., Guo, X.-D., et al. (2018). Improving cycling performance and rate capability of Ni-rich LiNi0. 8Co0. 1Mn0. 1O2 cathode materials by Li4Ti5O12 coating. *Electrochimica Acta* 268, 358–365. doi:10.1016/j.electacta.2018.02.049

Yang, H., Zhuang, G. V., and Ross, P. N., Jr (2006). Thermal stability of LiPF6 salt and Li-ion battery electrolytes containing LiPF6. *J. Power Sources* 161 (1), 573–579. doi:10.1016/j.jpowsour.2006.03.058

Yang, K., Fan, L.-Z., Guo, J., and Qu, X. (2012). Significant improvement of electrochemical properties of AlF3-coated LiNi0. 5Co0. 2Mn0. 3O2 cathode materials. *Electrochimica Acta* 63, 363–368. doi:10.1016/j.electacta.2011.12.121

Yu, H., Gao, Y., Kirtley, J., Borgmeyer, G., He, X., and Liang, X. (2022). Recovery of degraded Ni-rich NMC811 particles for lithium-ion batteries. *J. Electrochem. Soc.* 169 (5), 050520. doi:10.1149/1945-7111/ac6c56

Zhang, H., Xu, J., and Zhang, J. (2019). Surface-coated LiNi0. 8Co0. 1Mn0. 1O2 (NCM811) cathode materials by Al2O3, ZrO2, and Li2O-2B2O3 thin-layers for improving the performance of lithium ion batteries. *Front. Material* 6, 309. doi:10.3389/fmats.2019.00309

Zhang, J., Gao, R., Sun, L., Zhang, H., Hu, Z., and Liu, X. (2016). Unraveling the multiple effects of Li2ZrO3 coating on the structural and electrochemical performances of LiCoO2 as high-voltage cathode materials. *Electrochimica Acta* 209, 102–110. doi:10.1016/j.electacta.2016.05.066

Zou, P., Lin, Z., Fan, M., Wang, F., Liu, Y., and Xiong, X. (2020). Facile and efficient fabrication of Li3PO4-coated Ni-rich cathode for high-performance lithium-ion battery. *Appl. Surf. Sci.* 504, 144506. doi:10.1016/j.apsusc.2019.144506